

1 **On the Choice of Average Solar Zenith Angle**

2 TIMOTHY W. CRONIN *

Program in Atmospheres, Oceans, and Climate, Massachusetts Institute of Technology, Cambridge, Massachusetts

* *Corresponding author address:* MIT, 77 Massachusetts Ave., Cambridge, MA 02139.

E-mail: twcronin@mit.edu

ABSTRACT

3
4 Idealized climate modeling studies often choose to neglect spatiotemporal variations in so-
5 lar radiation, but doing so comes with an important decision about how to average solar
6 radiation in space and time. Since both clear-sky and cloud albedo are increasing functions
7 of the solar zenith angle, one can choose an absorption-weighted zenith angle which repro-
8 duces the spatial- or time-mean absorbed solar radiation. Here, we perform calculations
9 for a pure scattering atmosphere and with a more detailed radiative transfer model, and
10 find that the absorption-weighted zenith angle is usually between the daytime-weighted and
11 insolation-weighted zenith angles, but much closer to the insolation-weighted zenith angle in
12 most cases, especially if clouds are responsible for much of the shortwave reflection. Use of
13 daytime-average zenith angle may lead to a high bias in planetary albedo of $\sim 3\%$, equivalent
14 to a deficit in shortwave absorption of $\sim 10 \text{ W m}^{-2}$ in the global energy budget (comparable
15 to the radiative forcing of a roughly sixfold change in CO_2 concentration). Other studies that
16 have used general circulation models with spatially constant insolation have underestimated
17 the global-mean zenith angle, with a consequent low bias in planetary albedo of $\sim 2\text{-}6\%$, or
18 a surplus in shortwave absorption of $\sim 7\text{-}20 \text{ W m}^{-2}$ in the global energy budget.

1. Introduction

Comprehensive climate models suggest that a global increase in absorbed solar radiation by 1 W m^{-2} would lead to an $0.6\text{-}1.1 \text{ }^\circ\text{C}$ increase in global-mean surface temperatures (Soden and Held 2006). The amount of solar radiation absorbed or reflected by the Earth depends on the solar zenith angle (ζ), or angle the sun makes with a line perpendicular to the surface. When the sun is low in the sky (high ζ), much of the incident sunlight may be reflected even for a clear sky; when the sun is high in the sky (low ζ), even thick clouds may not reflect most of the incident sunlight. The difference in average zenith angle between the equator and poles is an important reason why the albedo is typically higher at high latitudes.

In order to simulate the average climate of a planet in radiative-convective equilibrium, one must globally average the incident solar radiation, and define either a solar zenith angle which is constant in time, or which varies diurnally (i.e., the sun rising and setting). The top-of-atmosphere incident solar radiation per unit ground area, or insolation I , is simply the product of the solar constant S_0 and the cosine of the solar zenith angle, $\mu \equiv \cos \zeta$:

$$I = S_0 \cos \zeta, \tag{1}$$

where the planetary-mean insolation is simply $\langle I \rangle = S_0/4 \approx 342 \text{ W m}^{-2}$ (in this paper, we will denote spatial averages with $\langle x \rangle$ and time averages with \bar{x}). A global-average radiative transfer calculation requires specifying both an effective cosine of solar zenith angle μ^* , and an effective solar constant, S_0^* , such that the resulting insolation matches the planetary-mean insolation:

$$\langle I \rangle = S_0/4 = S_0^* \mu^*. \tag{2}$$

Matching the mean insolation constrains only the product $S_0^* \mu^*$, and not either parameter individually, so additional assumptions are needed.

The details of these additional assumptions are quite important to simulated climate, because radiative transfer processes, most importantly cloud albedo, depend on μ (e.g., Hartmann (1994)). For instance, the most straightforward choice for a planetary-average

43 calculation might seem to be a simple average of μ over the whole planet, including the dark
 44 half, so that $S_{0S}^* = S_0$ and $\mu_S^* = 1/4$. However, this simple average would correspond to a sun
 45 that was always near setting, only $\sim 15^\circ$ above the horizon; with such a low sun, the albedo
 46 of clouds and the reflection by clear-sky Rayleigh scattering would be highly exaggerated.
 47 A more thoughtful, and widely used choice, is to ignore the contribution of the dark half of
 48 the planet to the average zenith angle. With this choice of daytime-weighted zenith angle,
 49 $\mu_D^* = 1/2$, and $S_{0D}^* = S_0/2$.

50 A slightly more complex option is to calculate the insolation-weighted cosine of the zenith
 51 angle, μ_I^* :

$$\mu_I^* = \frac{\int \mu S_0 \mu P(\mu) d\mu}{\int S_0 \mu P(\mu) d\mu}, \quad (3)$$

52 where $P(\mu)$ is the probability distribution function of global surface area as a function of the
 53 cosine of the zenith angle, μ , over the illuminated hemisphere. For the purposes of a planetary
 54 average, $P(\mu)$ simply equals 1. This can be seen by rotating coordinates so that the north
 55 pole is aligned with the subsolar point, where $\mu = 1$; then μ is given by the sine of the latitude
 56 over the illuminated northern hemisphere, and since area is uniformly distributed in the sine
 57 of the latitude, it follows that area is uniformly distributed over all values of μ between 0
 58 and 1. Hereafter, when discussing planetary averages, it should be understood that integrals
 59 over μ implicitly contain the probability distribution function $P(\mu) = 1$. Evaluation of (3)
 60 gives $\mu_I^* = 2/3$, and $S_{0I}^* = 3S_0/8$. Since most of the sunlight falling on the daytime hemisphere
 61 occurs where the sun is high, μ_I^* is considerably larger than μ_D^* . A schematic comparison
 62 of these three different choices – simple average, daytime-weighted, and insolation-weighted
 63 zenith angles – is given in Figure 1.

64 The daytime-average cosine zenith angle of 0.5 has been widely used. The early studies
 65 of radiative-convective equilibrium by *Manabe and Strickler* (1964), *Manabe and Wetherald*
 66 (1967), *Ramanathan* (1976), and the early review paper by *Ramanathan and Coakley* (1978),
 67 all took $\mu^* = 0.5$. The daytime-average zenith angle has also been used in simulation of
 68 climate on other planets (e.g., *Wordsworth et al.* (2010)), as well as estimation of global

69 radiative forcing by clouds and aerosols (*Fu and Liou* 1993; *Zhang et al.* 2013).

70 To our knowledge, no studies of global-mean climate with radiative-convective equilib-
71 rium models have used an insolation-weighted cosine zenith angle of $2/3$. The above consid-
72 erations regarding the spatial averaging of insolation, however, also apply to the temporal
73 averaging of insolation that is required to represent the diurnal cycle, or combined diurnal
74 and annual cycles, with a zenith angle that is constant in time. In this context, *Hartmann*
75 (1994) strongly argues for the use of insolation-weighted zenith angle, and provides a figure
76 with appropriate daily-mean insolation-weighted zenith angles as a function of latitude for
77 the solstices and the equinoxes (see *Hartmann* (1994), Figure 2.8). *Romps* (2011) also uses
78 an equatorial insolation-weighted zenith angle in a study of radiative-convective equilibrium
79 with a cloud-resolving model, though other studies of tropical radiative-convective equilib-
80 rium with cloud-resolving models, such as the work by *Tompkins and Craig* (1998), have used
81 a daytime-weighted zenith angle. In large-eddy simulations of marine low clouds, *Bretherton*
82 *et al.* (2013) advocate for the greater accuracy of the insolation-weighted zenith angle, noting
83 that the use of daytime-weighted zenith angle gives a 20 W m^{-2} stronger negative shortwave
84 cloud radiative effect than the insolation-weighted zenith angle. Biases of such a magnitude
85 would be especially disconcerting for situations where the surface temperature is interactive,
86 as they could lead to dramatic biases in mean temperatures.

87 Whether averaging in space or time, an objective decision of whether to use daytime-
88 weighted or insolation-weighted zenith angle requires some known and unbiased reference
89 point. In section 2, we develop the idea of absorption-weighted zenith angle as such an un-
90 biased reference point. We show that if albedo depends nearly linearly on the zenith angle,
91 which is true if clouds play a dominant role in solar reflection, then the insolation-weighted
92 zenith angle is likely to be less biased than the daytime-weighted zenith angle. We then
93 calculate the planetary-average absorption-weighted zenith angle for the extremely idealized
94 case of a purely conservative scattering atmosphere. In section 3, we perform calculations
95 with a more detailed shortwave radiative transfer model, and show that differences in plan-

96 etary albedo between $\mu_D^*=1/2$ and $\mu_I^* = 2/3$ can be $\sim 3\%$, equivalent to a radiative forcing
 97 difference of over 10 W m^{-2} . In section 4 we show that the superiority of insolation-weighting
 98 also applies for diurnally- or annually-averaged insolation. Finally, in section 5, we discuss
 99 the implications of our findings for recent studies with global models.

100 2. Absorption-Weighted Zenith Angle

101 For the purposes of minimizing biases in solar absorption, the zenith angle should be
 102 chosen to most closely match the spatial- or time-mean albedo. By this, we do not intend
 103 that the zenith angle should be tuned so as to match the observed albedo over a specific
 104 region or time period; rather, we wish to formulate a precise geometric closure on (2). If the
 105 albedo is a known function of the zenith angle (i.e., $\alpha = f_\alpha(\mu) = f_\alpha(\cos \zeta)$), then we can
 106 choose a zenith angle, μ_A^* , such that its albedo matches the albedo that would be calculated
 107 from a full average over space or time (as weighted by the probability density function $P(\mu)$):

$$f_\alpha(\mu_A^*) \int S_0 \mu P(\mu) d\mu = \int S_0 \mu f_\alpha(\mu) P(\mu) d\mu \quad (4)$$

108 If the albedo function f_α is smooth and monotonic in the zenith angle – the likely (albeit
 109 not universal) case for planetary reflection – then f_α can be inverted, and the problem is
 110 well-posed, with a unique solution:

$$\mu_A^* = f_\alpha^{-1} \left[\frac{\int \mu f_\alpha(\mu) P(\mu) d\mu}{\int \mu P(\mu) d\mu} \right], \quad (5)$$

111 where f_α^{-1} represents the inverse function of f_α . For the case of planetary-average solar
 112 absorption, the probability density function of μ over the sunlit half of the globe is uniform
 113 (see discussion following equation (3)). Taking $P(\mu) = 1$, equation (5) simplifies to:

$$\langle \alpha \rangle = 2 \int_0^1 \mu f_\alpha(\mu) d\mu, \quad (6)$$

$$\mu_A^* = f_\alpha^{-1} \left[2 \int_0^1 \mu f_\alpha(\mu) d\mu \right], \quad (7)$$

114 where $\langle \alpha \rangle$ is the planetary albedo, or ratio of reflected to incident global shortwave radiation.
 115 Note that a bias in planetary albedo by 1% would lead to a bias in planetary-average absorbed
 116 shortwave radiation of 3.42 W m^{-2} .

117 If the albedo is a linear function of the zenith angle, we can write:

$$f_\alpha(\mu) = \alpha_{\max} - \alpha_\Delta \mu, \quad (8)$$

118 where α_{\max} is the maximum albedo (for $\mu = 0$), and α_Δ is the drop in albedo in going from
 119 $\mu = 0$ to $\mu = 1$. In this case, we can show that the absorption-weighted zenith angle is
 120 exactly equal to the insolation-weighted zenith angle, regardless of the form of $P(\mu)$. From
 121 (3), (4), and (8), it follows that:

$$\begin{aligned} \alpha_{\max} \int \mu P(\mu) d\mu - \alpha_\Delta \mu_A^* \int \mu P(\mu) d\mu &= \alpha_{\max} \int \mu P(\mu) d\mu - \alpha_\Delta \int \mu^2 P(\mu) d\mu \\ \mu_A^* &= \frac{\int \mu^2 P(\mu) d\mu}{\int \mu P(\mu) d\mu} = \mu_I^*. \end{aligned} \quad (9)$$

122 Thus, if the albedo varies roughly linearly with μ , then we expect the insolation-weighted
 123 zenith angle to closely match the absorption-weighted zenith angle.

124 For planetary-average solar absorption, the simplicity of $P(\mu)$ allows us to perform an
 125 additional analytic calculation of the absorption-weighted zenith angle. Consider an albedo
 126 similar to (8), but which may now vary nonlinearly, as some power of the cosine of the zenith
 127 angle:

$$f_\alpha(\mu) = \alpha_{\max} - \alpha_\Delta \mu^b. \quad (10)$$

128 The power b is likely equal to or less than 1, so that the albedo is more sensitive to the zenith
 129 angle when the sun is low than when the sun is high. For a general value of b , the planetary
 130 albedo and absorption-weighted zenith angle are given by:

$$\begin{aligned} \langle \alpha \rangle &= \alpha_{\max} - \frac{\alpha_\Delta}{1 + b/2} \\ \mu_A^* &= \left(\frac{1}{1 + b/2} \right)^{1/b}. \end{aligned} \quad (11)$$

131 As noted above, if the albedo depends linearly on μ ($b=1$), then the absorption-weighted
 132 zenith angle has a cosine of $2/3$, which is equal to planetary-average value of the insolation-
 133 weighted cosine zenith angle (μ_I^*). For $0 < b < 1$, μ_A^* always falls between $e^{-1/2} \approx 0.607$ and
 134 $2/3$, suggesting that $\mu_I^* = 2/3$ is generally a good choice for the zenith angle in planetary-
 135 mean calculations. The albedo must be a strongly nonlinear function of μ , with significant
 136 weight at low μ , in order to obtain values of $\mu_A^* < 0.6$.

137 *a. Example: A Pure Scattering Atmosphere*

138 How strongly does the planetary albedo depend on μ for a less idealized function $f_\alpha(\mu)$?
 139 For a pure conservative scattering atmosphere, with optical thickness τ^* , two-stream coef-
 140 ficient γ (which we will take $=3/4$, corresponding to the Eddington approximation (*Pier-*
 141 *rehumbert* 2010)), and scattering asymmetry parameter \hat{g} , equation 5.38 of *Pierrehumbert*
 142 (2010) gives the atmospheric albedo as:

$$\alpha_a = \frac{(1/2 - \gamma\mu)(1 - e^{-\tau^*/\mu}) + (1 - \hat{g})\gamma\tau^*}{1 + (1 - \hat{g})\gamma\tau^*}. \quad (12)$$

143 Defining a constant surface albedo of α_g , and a diffuse atmospheric albedo α'_a , the total
 144 albedo is:

$$\alpha = 1 - \frac{(1 - \alpha_g)(1 - \alpha_a)}{(1 - \alpha_g)\alpha'_a + (1 - \alpha'_a)}. \quad (13)$$

145 Using this expression, we can calculate how the albedo depends on zenith angle for different
 146 sky conditions. Figure 2 shows the dependence of the albedo on the cosine of the solar
 147 zenith angle, for a case of Rayleigh scattering by the clear sky ($\tau^* \approx 0.12$, $\hat{g} = 0$), for a
 148 cloudy-sky example ($\tau^* = 3.92$, $\hat{g} = 0.843$), and for a linear mix of 68.6 % cloudy and
 149 31.4 % clear sky, which is roughly the observed cloud fraction as measured by satellites
 150 (*Rossow and Schiffer* 1999). Values of average cloud optical thickness are taken from *Rossow*
 151 *and Schiffer* (1999), with the optical thickness equal to the sum of cloud and Rayleigh
 152 scattering optical thicknesses (3.8 and 0.12, respectively), and the asymmetry parameter set
 153 to a weighted average of cloud and Rayleigh scattering asymmetry parameters (0.87 and 0,

154 respectively). Figure 2 also shows the appropriate choice of the cosine of the absorption-
 155 weighted zenith angle, μ_A^* , for the clear and cloudy-sky examples. The clear-sky case has
 156 $\mu_A^* = 0.55$, the cloudy-sky case has $\mu_A^* = 0.665$, and the mixed-sky case has $\mu_A^* = 0.653$.
 157 In these calculations, and others throughout the paper, we have fixed the surface albedo
 158 to a constant of 0.12, independent of μ , in order to focus on the atmospheric contribution
 159 to planetary reflection. The particular surface albedo value of 0.12 is chosen following the
 160 observed global mean surface reflectance from Figure 5 of *Donohoe and Battisti* (2011)
 161 (average of the hemispheric values from observations). Of course, surface reflection also
 162 generally depends on μ , with the direct-beam albedo increasing at lower μ , but surface
 163 reflection plays a relatively minor role in planetary albedo, in part because so much of the
 164 Earth is covered by clouds (*Donohoe and Battisti* 2011).

165 We can also use these results to calculate what bias would result from the use of the
 166 daytime-weighted zenith angle ($\mu_D^*=1/2$) or the insolation-weighted zenith angle ($\mu_I^*=2/3$).
 167 The planetary albedo is generally overestimated by use of μ_D^* and underestimated by use of
 168 μ_I^* ; the first three rows of Table 1 summarize our findings for a pure scattering atmosphere.
 169 For a clear sky, the daytime-weighted zenith angle is a slightly more accurate choice than
 170 the insolation-weighted zenith angle. On the other hand, for a cloudy sky with moderate
 171 optical thickness, the insolation-weighted zenith angle is essentially exact, and a daytime-
 172 weighted zenith angle may overestimate the planetary albedo by over 7%. For Earthlike
 173 conditions, with a mixed sky that has low optical thickness in clear regions, and moderate
 174 optical thickness in cloudy regions, a cosine-zenith angle close to but slightly less than the
 175 planetary insolation-weighted mean value of $2/3$ is likely the best choice. The common
 176 choice of $\mu^* = 1/2$ will overestimate the negative shortwave radiative effect of clouds, while
 177 choices of $\mu^* > 2/3$ will underestimate the negative shortwave radiative effect of clouds.
 178 Our calculations here, however, are quite simplistic, and do not account for atmospheric
 179 absorption or wavelength-dependence of optical properties. In the following section, we will
 180 use a more detailed model to support the assertion that the insolation-weighted zenith angle

181 leads to smaller albedo biases than the daytime-weighted zenith angle.

182 **3. Calculations with a Full Radiative Transfer Model**

183 The above calculations provide a sense for the magnitude of planetary albedo bias that
184 may result from different choices of average solar zenith angle. In this section, we calculate
185 albedos using version 3.8 of the shortwave portion of the Rapid Radiative Transfer Model,
186 for application to GCMs (RRTMG_SW, v3.8; *Iacono et al. (2008)*; *Clough et al. (2005)*);
187 hereafter we refer to this model as simply “RRTM” for brevity. Calculations with RRTM
188 allow for estimation of biases associated with different choices of μ when the atmosphere has
189 more realistic scattering and absorption properties than we assumed in the pure scattering
190 expressions above ((12), (13)). RRTM is a broadband, two-stream, correlated k-distribution
191 radiative transfer model, which has been tested against line-by-line radiative transfer models,
192 and is used in several general circulation models (GCMs). For calculation of radiative fluxes
193 in partly cloudy skies, the model uses the Monte-Carlo independent column approximation
194 (McICA; *Pincus et al. (2003)*), which stochastically samples 200 profiles over the possible
195 range of combinations of cloud overlap arising from prescribed clouds at different vertical
196 levels, and averages the fluxes that result.

197 We use RRTM to calculate the albedo as a function of zenith angle for a set of built-
198 in reference atmospheric profiles, and several cloud profile assumptions. The atmospheric
199 profiles we use are the Tropical atmosphere, the 1976 U.S. Standard Atmosphere, and the
200 Subarctic Winter atmosphere, and we perform calculations with clear skies, as well as two
201 cloud profile assumptions (Table 2). One cloud profile is a mixed sky, intended to mirror
202 Earth’s climatological cloud distribution, with four cloud layers having fractional coverage,
203 water path, and altitudes based *Rossow and Schiffer (1999)*; we call this case “RS99”. The
204 other cloud profile is simply fully overcast with a low-level “Stratocumulus” cloud deck,
205 having a water path of 100 g/m². Table 2 gives the values for assumed cloud fractions,

206 altitudes, and in-cloud average liquid and ice water in clouds at each level. Cloud fractions
 207 have been modified from Table 4 of *Rossow and Schiffer* (1999) because satellites see clouds
 208 from above, and will underestimate true low cloud fraction that is overlain by higher clouds.
 209 If multiple cloud layers are randomly overlapping, and seen from above, then, indexing cloud
 210 layers as (1,2,...) from the top down, we denote $\hat{\sigma}_i$ as the observed cloud fraction in layer i ,
 211 and σ_i as the true cloud fraction in layer i . The true cloud fraction in layer i is:

$$\sigma_i = \hat{\sigma}_i \left(1 - \sum_{j=1}^{i-1} \hat{\sigma}_j \right)^{-1}, \quad (14)$$

212 which can be seen because the summation gives the fraction of observed cloudy sky above
 213 level i , so the term in parentheses gives the fraction of clear sky above level i , which is equal to
 214 the ratio of observed cloud fraction to true cloud fraction in layer i (again assuming random
 215 cloud overlap). Applying this correction to observed cloud fractions $(\hat{\sigma}_1, \hat{\sigma}_2, \hat{\sigma}_3, \hat{\sigma}_4)=(0.196,$
 216 $0.026, 0.190, 0.275)$ from Table 4 of *Rossow and Schiffer* (1999) gives the cloud fractions
 217 listed in Table 2: $(\sigma_1, \sigma_2, \sigma_3, \sigma_4)=(0.196, 0.032, 0.244, 0.467)$.

218 To isolate the contributions from changing atmospheric (and especially cloud) albedo as
 219 a function of μ , the surface albedo is set to a value of 0.12 for all calculations, independent of
 220 the solar zenith angle. Using RRTM calculations of albedo at 22 roughly evenly-spaced values
 221 of μ , we interpolate $f_\alpha(\mu)$ to a grid in μ with spacing 0.001, calculate the planetary albedo
 222 $\langle\alpha\rangle$ from equation (6), and find the value of μ_A^* whose albedo most closely matches $\langle\alpha\rangle$. The
 223 dependence of albedo on μ is shown in Figure 3; atmospheric absorption results in generally
 224 lower values of albedo than in the pure scattering cases above, as well as lower sensitivity
 225 of the albedo to zenith angle. For partly or fully cloudy skies, the albedo is approximately
 226 linear in the zenith angle. Note that $f_\alpha(\mu)$ here is not necessarily monotonic, as it decreases
 227 for very small μ . This implies that the inverse problem can return two solutions for μ_A^* in
 228 some cases; we select the larger result if this occurs.

229 For clear skies, biases in $\langle\alpha\rangle$ are nearly equal in magnitude for μ_D^* and μ_I^* (Table 1). For
 230 partly cloudy or overcast skies, however, biases in $\langle\alpha\rangle$ are much larger for μ_D^* than for μ_I^* ; the

231 insolation-weighted zenith angle has an albedo bias that is lower by an order of magnitude
 232 than the albedo bias of the daytime-weighted zenith angle. The bias in solar absorption for
 233 partly-cloudy or overcast skies for μ_D^* is on the order of 10 W m^{-2} . While we have only
 234 tabulated biases for the 1976 U.S. Standard Atmosphere, results are similar across other
 235 reference atmospheric profiles.

236 4. Diurnal and Annual Averaging

237 Thus far, we have presented examples of albedo biases only for the case of planetary-mean
 238 calculations. The absorption-weighted zenith angle can also be calculated and compared to
 239 daytime-weighted and insolation-weighted zenith angles for the case of diurnal- or annual-
 240 average solar radiation at a single point on the Earth’s surface, using (5). The latitude and
 241 temporal averaging period both enter into the calculation of the probability density function
 242 $P(\mu)$, as well as the bounds of the integrals in (5). We will look at how μ_A^* varies as a
 243 function of latitude for two cases: an equinoctial diurnal cycle and a full average over annual
 244 and diurnal cycles. In both cases, we will use $f_\alpha(\mu)$ as calculated by RRTM, for the 1976
 245 U.S. Standard Atmosphere, and the mixed-sky cloud profile of RS99.

246 For an equinoctial diurnal cycle at latitude ϕ , the cosine of the zenith angle is given by
 247 $\mu(h) = \cos \phi \cos(\pi(h - 12)/12)$, where h is the local solar time in hours. Since time (h) is
 248 uniformly distributed, this can be analytically transformed to obtain the probability density
 249 function $P(\mu)$:

$$P(\mu) = \frac{2}{\pi \sqrt{\cos^2 \phi - \mu^2}}, \quad (15)$$

250 which is valid for $0 \leq \mu < \cos \phi$. For the equinoctial diurnal cycle, daytime-weighting gives
 251 $\mu_D^* = (2/\pi) \cos \phi$, while insolation-weighting gives $\mu_I^* = (\pi/4) \cos \phi$. Figure 4 shows that the
 252 absorption-weighted zenith angle is once again much closer to the insolation-weighted zenith
 253 angle than to the daytime-weighted zenith angle for partly cloudy skies. We can also look at
 254 how the time-mean albedo $\bar{\alpha}$ compares to the albedo calculated from μ_D^* or μ_I^* . Albedo biases

255 at the equator are -0.2% for insolation-weighting, and +2.6% for daytime-weighting, which
256 translates to solar absorption biases of +0.9 W m⁻² and -11.2 W m⁻², respectively. For
257 clear-sky calculations (not shown), results are also similar to what we found for planetary-
258 average calculations: the two choices are almost equally biased, with albedo underestimated
259 by ~0.5% when using μ_I^* , and overestimated by ~0.5% when using μ_D^* .

260 For the full annual and diurnal cycles of insolation, $P(\mu)$ must be numerically tabu-
261 lated. For each latitude band, we calculate μ every minute over a year, and construct $P(\mu)$
262 histograms with bin width 0.001 in μ , then we calculate the insolation-weighted, daytime-
263 weighted, and absorption weighted cosine zenith angles and corresponding albedos (Figure
264 5). For partly cloudy skies, the insolation-weighted zenith angle is a good match to the
265 absorption-weighted zenith angle, with biases in albedo of less than 0.2%. Albedo biases for
266 the daytime-weighted zenith angle are generally ~2-3%, with a maximum of over 3% around
267 60 degrees latitude. The solar absorption biases at the equator are similar to those found in
268 the equinoctial diurnal average, though slightly smaller. Overall, these findings indicate that
269 insolation-weighting is generally a better approach than daytime-weighting for representing
270 annual or diurnal variations in insolation.

271 5. Discussion

272 The work presented here addresses potential climate biases in two major lines of inquiry in
273 climate science. One is the use of radiative-convective equilibrium, either in single-column or
274 small-domain cloud resolving models, as a framework to simulate and understand important
275 aspects of planetary-mean climate, such as surface temperature and precipitation. The
276 second is the increasing use of idealized three-dimensional general circulation models (GCMs)
277 for understanding large-scale atmospheric dynamics. Both of these categories span a broad
278 range of topics, from understanding the limits of the circumstellar habitable zone and the
279 scaling of global-mean precipitation with temperature in the case of radiative-convective

280 models, to the location of midlatitude storm tracks and the strength of the Hadley circulation
281 in the case of idealized GCMs. Both categories of model often sensibly choose to ignore
282 diurnal and annual variations in insolation, so as to reduce simulation times and avoid
283 unnecessary complexity. Our work suggests that spatial or temporal averaging of solar
284 radiation, however, can lead to biases in total absorbed solar radiation on the order of 10 W
285 m^{-2} , especially if the models used have a large cloud area fraction.

286 The extent to which a radiative-convective equilibrium model forced by global-average
287 insolation accurately captures the global-mean surface temperature of both the real Earth,
288 and more complex three-dimensional GCMs, is a key test of the magnitude of nonlinearities
289 in the climate system. For instance, variability in tropospheric relative humidity, as induced
290 by large-scale vertical motions in the tropics, can give rise to dry-atmosphere “radiator
291 fin” regions that emit longwave radiation to space more effectively than would a horizontally
292 uniform atmosphere, resulting in a cooling of global mean temperatures relative to a reference
293 atmosphere with homogeneous relative humidity (*Pierrehumbert* 1995). This “radiator fin”
294 nonlinearity can appear in radiative-convective equilibrium simulations with cloud-resolving
295 models as a result of self-aggregation of convection, with a large change in domain-average
296 properties such as relative humidity and outgoing longwave radiation (*Muller and Held* 2012;
297 *Wing and Emanuel* 2013). But many other potentially important climate nonlinearities –
298 such as the influence of ice on planetary albedo, interactions between clouds and large-
299 scale dynamics (including mid-latitude baroclinic eddies and the clouds they generate), and
300 rectification of spatiotemporal variability in lapse rates – would be quite difficult to plausibly
301 incorporate into a radiative-convective model. Thus, despite its simplicity, the question of
302 how important these and other climate nonlinearities are – in the sense of how much they
303 alter Earth’s mean temperature as compared to a hypothetical radiative-convective model
304 of Earth – remains a fundamental and unanswered question in climate science.

305 The recent work of *Popke et al.* (2013) is possibly the first credible stab at setting up
306 an answer to this broader question of the significance of climate nonlinearities. *Popke et al.*

307 (2013) use a global model (ECHAM6) with uniform insolation and no rotation to simu-
308 late planetary radiative-convective equilibrium with column physics over a slab ocean, thus
309 allowing for interactions between convection and circulations up to planetary scales. One
310 could imagine a set of simulations with this modeling framework where various climate non-
311 linearities were slowly dialed in. For example, simulations could be conducted across a range
312 of planetary rotation rates, as well as with a range of equator-to-pole insolation contrasts;
313 progressively stronger mid-latitude eddies would emerge from the interaction between in-
314 creasing rotation rate and increasing insolation gradients, and the influence of mid-latitude
315 dynamics on the mean temperature of the Earth could be diagnosed. But the study of *Popke*
316 *et al.* (2013) does not focus on comparing the mean state of their simulations to the mean
317 climate of the Earth; they find surface temperatures of ~ 28 °C, which are much warmer
318 than the observed global-mean surface temperature of ~ 14 °C. The combination of warm
319 temperatures and nonrotating dynamics prompts comparison of their simulated cloud and
320 relative humidity distributions to the Earth’s Tropics, where they find good agreement with
321 the regime-sorted cloud radiative effects in the observed tropical atmosphere.

322 The most obvious cause of the warmth of their simulations is that *Popke et al.* (2013)
323 also find an anomalously low planetary albedo of ~ 0.2 , much lower than Earth’s observed
324 value of 0.3 (e.g., *Hartmann* (1994)). Although part of the reason for this low albedo can
325 be readily explained by the low surface albedo of 0.07 in *Popke et al.* (2013), the remaining
326 discrepancy is large, in excess of 5% of planetary albedo. It is possible that this remaining
327 discrepancy arises principally due to the lack of bright clouds from mid-latitude storms. But
328 our study indicates that their use of a uniform equatorial equinox diurnal cycle of insolation,
329 with $\mu_I^* = \pi/4$, also contributes to the underestimation of both cloud and clear-sky albedo.
330 For RS99 clouds and an equatorial equinox diurnal cycle, we estimate a time-mean albedo
331 of 32.7%; the same cloud field would give a planetary albedo of 34.6% if the planetary-
332 average insolation-weighted cosine zenith angle of $2/3$ were used. In other words, if the
333 cloud distribution from *Popke et al.* (2013) were put on a realistically illuminated planet,

334 we estimate that the planetary albedo would be $\sim 2\%$ higher; the shortwave absorption in
335 *Popke et al.* (2013) may be biased by $\sim 6.7 \text{ W m}^{-2}$ due to zenith angle considerations alone.

336 Previous simulations by *Kirtman and Schneider* (2000), and *Barsugli et al.* (2005) also
337 found very warm global-mean temperatures when insolation contrasts were removed; plan-
338 etary rotation was retained in both studies. *Kirtman and Schneider* (2000) found a global-
339 mean surface temperature of $\sim 26 \text{ }^\circ\text{C}$ with a reduced global-mean insolation of only 315 W
340 m^{-2} ; realistic global-mean insolation led to too-warm temperatures and numerical instability.
341 *Kirtman and Schneider* (2000) offer little explanation for the extreme warmth of their sim-
342 ulations, but apparently also chose to homogenize insolation by using an equatorial equinox
343 diurnal cycle, with $\mu_I^* = \pi/4$. *Barsugli et al.* (2005) obtained a global-mean surface temper-
344 ature of $\sim 38 \text{ }^\circ\text{C}$ when using a realistic global-mean insolation of 340 W m^{-2} . Similarly to
345 *Popke et al.* (2013), *Barsugli et al.* (2005) also invoke a low planetary albedo of 0.21 as a
346 plausible reason for their global warmth, and explain their low albedo as a consequence of
347 a dark all-ocean surface. This work, however, suggests that their unphysical use of constant
348 $\mu=1$ may lead to a large albedo bias on its own. For RS99 clouds, we estimate an albedo
349 of 28.8% for $\mu=1$, as compared to 34.6% for $\mu=2/3$, so their albedo bias may be as large
350 as -5.8%, with a resulting shortwave absorption bias of $+19.8 \text{ W m}^{-2}$. Use of these three
351 studies (*Kirtman and Schneider* 2000; *Barsugli et al.* 2005; *Popke et al.* 2013) as a starting
352 point for questions about the importance of climate nonlinearities may thus be impeded by
353 biases in planetary albedo and temperature due to a sun that is too high in the sky. While it
354 was not the primary focus of these studies to query the importance of climate nonlinearities,
355 these studies nonetheless serve as a reminder that care is required when using idealized solar
356 geometry in models.

357 Because global-mean temperatures are quite sensitive to planetary albedo, we have fo-
358 cused in this work on matching the top-of-atmosphere shortwave absorption. For either a
359 radiative-convective model or a GCM, we expect biases in mean solar absorption to translate
360 cleanly to biases in mean temperature. The bias in mean temperature, T' , should scale with

361 the bias in solar absorption, R'_S (units: W m^{-2}), divided by the total feedback parameter
362 of the model, λ (units: $\text{W m}^{-2} \text{K}^{-1}$): $T' = R'_S/\lambda$. But matching the top-of-atmosphere
363 absorbed shortwave radiation does not guarantee unbiased partitioning into atmospheric
364 and surface absorption, although our method of bias minimization could be altered to match
365 some other quantity instead, such as the shortwave radiation absorbed by the surface. Based
366 on our calculations with RRTM, it appears that a single value of $\mu \sim 0.58$ will give both the
367 correct planetary albedo and the correct partitioning of absorbed shortwave radiation for
368 clear skies; however, for partly cloudy or overcast skies, a single value of μ cannot simultane-
369 ously match both the planetary albedo and the partitioning of absorbed shortwave radiation.
370 Together with the correspondence between global precipitation and free-tropospheric radia-
371 tive cooling (e.g., *Takahashi (2009)*), the dependence of atmospheric solar absorption on
372 zenith angle suggests that idealized simulations could obtain different relationships between
373 temperature and precipitation due solely to differences in solar zenith angle.

374 Finally, we note that the use of an appropriately-averaged solar zenith angle still has
375 obvious limitations. Any choice of insolation that is constant in time cannot hope to capture
376 any covariance between albedo and insolation, which might exist due to diurnal or annual
377 cycles of cloud fraction, height, or optical thickness. Furthermore, use of an absorption-
378 weighted zenith angle will do nothing to remedy model biases in cloud fraction or water
379 content that arise from the model's convection or cloud parameterizations. We hope that
380 the methodology and results introduced in this paper will mean that future studies make
381 better choices with regards to solar zenith angle averaging, and thus will not convolute real
382 biases in cloud properties with artificial biases in cloud radiative effects that are solely related
383 to zenith angle averaging.

384 *Acknowledgments.*

385 Thanks to Kerry Emanuel, Martin Singh, Aaron Donohoe, Peter Molnar, and Paul
386 O'Gorman for helpful conversations, and to Dennis Hartmann, Aiko Voigt, and one anyon-

387 mous reviewer for useful comments. This work was funded by NSF Grant 1136480, The
388 Effect of Near-Equatorial Islands on Climate.

REFERENCES

- 391 Barsugli, J., S. Shin, and P. Sardeshmukh, 2005: Tropical Climate Regimes and Global
392 Climate Sensitivity in a Simple Setting. *J. Atmos. Sci.*, **62**, 1226–1240.
- 393 Bretherton, C., P. Blossey, and C. Jones, 2013: Mechanisms of marine low cloud sensitivity
394 to idealized climate perturbations: A single-LES exploration extending the CGILS cases.
395 *J. Adv. Model. Earth Sys.*, **5**, 316–337, doi:10.1002/jame.20019.
- 396 Clough, S., M. Shephard, E. Mlawer, J. Delamere, M. Iacono, K. Cady-Pereira, S. Boukabara,
397 and P. Brown, 2005: Atmospheric radiative transfer modeling: a summary of the AER
398 codes. *J. Quant. Spectrosc. Radiat. Transfer*, **91**, 233–244.
- 399 Donohoe, A., and D. Battisti, 2011: Atmospheric and Surface Contributions to Planetary
400 Albedo. *J. Climate*, **24**, 4402–4418, doi:10.1175/2011JCLI3946.1.
- 401 Fu, Q., and K. Liou, 1993: Parameterization of the Radiative Properties of Cirrus Clouds.
402 *J. Atmos. Sci.*, **50**, 2008–2025.
- 403 Hartmann, D., 1994: *Global Physical Climatology*. Academic Press, International Geophysics
404 Series Volume 56, San Diego, 409 pp.
- 405 Iacono, M., J. Delamere, E. Mlawer, M. Shephard, S. Clough, and W. Collins, 2008: Radia-
406 tive forcing by long-lived greenhouse gases: Calculations with the AER radiative transfer
407 models. *J. Geophys. Res.*, **113**, D13103, doi:10.1029/2008JD009944.
- 408 Kirtman, B., and E. Schneider, 2000: A Spontaneously Generated Tropical Atmospheric
409 General Circulation. *J. Atmos. Sci.*, **57**, 2080–2093.
- 410 Manabe, S., and R. Strickler, 1964: Thermal equilibrium of the atmosphere with a convective
411 adjustment. *J. Atmos. Sci.*, **21**, 361–385.

- 412 Manabe, S., and R. Wetherald, 1967: Thermal equilibrium of the atmosphere with a given
413 distribution of relative humidity. *J. Atmos. Sci.*, **24**, 241–259.
- 414 Muller, C., and I. Held, 2012: Detailed Investigation of the Self-Aggregation of Convection
415 in Cloud-Resolving Simulations. *J. Atmos. Sci.*, **69**, 2551–2565, doi:10.1175/JAS-D-11-
416 0257.1.
- 417 Pierrehumbert, R., 1995: Thermostats, Radiator Fins, and the Local Runaway Greenhouse.
418 *J. Atmos. Sci.*, **52**, 1784–1806.
- 419 Pierrehumbert, R., 2010: *Principles of Planetary Climate*. Cambridge University Press,
420 Cambridge, UK, 652 pp.
- 421 Pincus, R., H. Barker, and J. Morcrette, 2003: A fast, flexible, approximation technique for
422 computing radiative transfer in inhomogeneous cloud fields. *J. Geophys. Res.*, **108**(D13),
423 4376, doi:10.1029/2002JD003322.
- 424 Popke, D., B. Stevens, and A. Voigt, 2013: Climate and Climate Change in a Radiative-
425 Convective Equilibrium Version of ECHAM6. *J. Adv. Model. Earth Sys.*, **5**, 1–14,
426 doi:10.1029/2012MS000191.
- 427 Ramanathan, V., 1976: Radiative Transfer Within the Earth’s Troposphere and Strato-
428 sphere: A Simplified Radiative-Convective Model. *J. Atmos. Sci.*, **33**, 1330–1346.
- 429 Ramanathan, V., and J. Coakley, 1978: Climate Modeling Through Radiative-Convective
430 Models. *Reviews of Geophysics and Space Physics*, **16**, 465–489.
- 431 Romps, D., 2011: Response of Tropical Precipitation to Global Warming. *J. Atmos. Sci.*,
432 **68**, 123–138, doi:10.1175/2010JAS3542.1.
- 433 Rossow, W., and R. Schiffer, 1999: Advances in Understanding Clouds from ISCCP. *Bull.*
434 *Amer. Meteor. Soc.*, **80**, 2261–2287.

- 435 Soden, B., and I. Held, 2006: An assessment of climate feedbacks in coupled ocean-
436 atmosphere models. *J. Climate*, **19**, 3354-3360, doi:10.1175/JCLI3799.1.
- 437 Takahashi, K., 2009: Radiative constraints on the hydrological cycle in an idealized radiative-
438 convective equilibrium model. *J. Atmos. Sci.*, **66**, 77-91, doi:10.1175/2008JAS2797.1.
- 439 Tompkins, A., and G. Craig, 1998: Radiative-convective equilibrium in a three-dimensional
440 cloud-ensemble model. *Quart. J. Roy. Meteor. Soc.*, **124**, 2073-2097.
- 441 Wing, A., and K. Emanuel, 2014: Physical mechanisms controlling self-aggregation of con-
442 vection in idealized numerical modeling simulations. *J. Adv. Model. Earth Sys.*, **5**, 1-14,
443 doi:10.1002/2013MS000269.
- 444 Wordsworth, R., F. Forget, F. Selsis, J. Madeleine, E. Millour, and V. Eymet, 2010: Is Gliese
445 581d habitable? Some constraints from radiative-convective climate modeling. *Astron.*
446 *Astrophys.*, **522**, A22, doi: 10.1051/0004-6361/201015053.
- 447 Zhang, L., Q. Li, Y. Gu, K. Liou, and B. Meland, 2013: Dust vertical profile impact on
448 global radiative forcing estimation using a coupled chemical-transport-radiative-transfer
449 model. *Atmos. Chem. Phys.*, **13**, 7097-7114, doi:10.5194/acp-13-7097-2013.

450 List of Tables

451	1	Table of planetary albedos and biases.	22
452	2	Cloud profiles used in calculations with RRTM. The multiple cloud layers	
453		of <i>Rossow and Schiffer</i> (1999) are used together, and are assumed to over-	
454		lap randomly. Cloud fractions are based on Table 4 of <i>Rossow and Schiffer</i>	
455		(1999), but adjusted for random overlap and observation from above (see	
456		text). Cloud-top altitudes are based on top pressures from <i>Rossow and Schif-</i>	
457		<i>fer</i> (1999) and pressure-height profile from 1976 U.S. Standard Atmosphere.	
458		Cloud water/ice allocation uses 260 K as a threshold temperature.	23

TABLE 1. Table of planetary albedos and biases.

Radiative Transfer Model	Atmospheric Profile	$\langle\alpha\rangle$	μ_A^*	Biases in α (%)	
		(%)		$\mu=1/2$	$\mu=2/3$
Pure scattering	clear sky	19.9	0.550	0.78	-1.40
Pure scattering	68.6% ISCCP cloud, 31.4% clear	31.9	0.653	5.57	-0.49
Pure scattering	ISCCP cloud	37.4	0.665	7.77	-0.08
RRTM	1976 U.S. Standard - clear	14.1	0.576	0.56	-0.53
RRTM	1976 U.S. Standard - RS99 clouds	34.8	0.657	3.16	-0.19
RRTM	1976 U.S. Standard - Stratocumulus	51.5	0.686	3.53	0.37

TABLE 2. Cloud profiles used in calculations with RRTM. The multiple cloud layers of *Rossow and Schiffer* (1999) are used together, and are assumed to overlap randomly. Cloud fractions are based on Table 4 of *Rossow and Schiffer* (1999), but adjusted for random overlap and observation from above (see text). Cloud-top altitudes are based on top pressures from *Rossow and Schiffer* (1999) and pressure-height profile from 1976 U.S. Standard Atmosphere. Cloud water/ice allocation uses 260 K as a threshold temperature.

Cloud Profile	fraction (-)	top altitude (km)	water path (g/m ²)	ice path (g/m ²)
<i>Rossow and Schiffer</i> (1999) RS99 low	0.475	2	51	0
<i>Rossow and Schiffer</i> (1999) RS99 medium	0.244	5	0	60
<i>Rossow and Schiffer</i> (1999) RS99 convective	0.032	9	0	261
<i>Rossow and Schiffer</i> (1999) RS99 cirrus	0.196	10.5	0	23
Stratocumulus	1.0	2	100	0

459 List of Figures

- 460 1 Schematic example of three different choices of zenith angle and solar constant
461 that give the same insolation. The solar zenith angle ζ is shown for each of
462 the three choices, which correspond to simple average, daytime-weighted, and
463 insolation-weighted choices of μ , as in the text. 26
- 464 2 Plot of albedo against cosine of the zenith angle, for a pure conservative scat-
465 tering atmospheric column, based on *Pierrehumbert* (2010), equation (5.41).
466 We show calculations for a clear-sky case with $\tau^*=0.12$ and $\hat{g}=0$ (blue), for a
467 cloudy case, with $\tau^*=3.92$ and $\hat{g}=0.843$ (gray), and a linear mix of the two for
468 a sky that is 68.6 % cloudy and 31.4 % clear (blue-gray). The average cloud
469 fraction and optical thickness are taken after International Satellite Cloud Cli-
470 matology Project (ISCCP) measurements (*Rossow and Schiffer* 1999), and the
471 surface albedo is set to a constant of 0.12, independent of μ . The values of the
472 cosines of absorption-weighted zenith angle are indicated by the x-locations
473 of the vertical dotted lines, and the planetary-average albedos are indicated
474 by the y-locations of the horizontal dotted lines (see also Table 1). 27
- 475 3 Plot of albedo against cosine of the zenith angle, for calculations from RRTM.
476 Albedo is shown for three atmospheric profiles: Tropical (red), 1976 U.S. Stan-
477 dard (green), and Subarctic winter (blue). We also show results for clear-sky
478 radiative transfer (bottom set of lines), as well two cloud profile assumptions:
479 observed RS99 cloud climatology (middle set of lines), and Stratocumulus
480 overcast (upper set of lines) – see Table 2 for more details on cloud assump-
481 tions. The surface albedo is set to a constant of 0.12 in all cases, independent
482 of μ . 28

- 483 4 Plot of diurnal-average zenith angles (top), and biases in time-mean albedo
484 (bottom) for equinoctial diurnal cycles, as a function of latitude. Albedo is
485 calculated in RRTM, using the 1976 U.S. Standard Atmosphere and RS99
486 clouds (Table 2). Albedo biases for the daytime-weighted zenith angle (μ_D^* ,
487 red) and the insolation-weighted zenith angle (μ_I^* , blue) are calculated relative
488 to the absorption-weighted zenith angle (μ_A^* , black). 29
- 489 5 Plot of annual-average zenith angles (top), and biases in time-mean albedo
490 (bottom) for full annual and diurnal cycles of insolation, as a function of
491 latitude. Albedo is calculated in RRTM, using the 1976 U.S. Standard Atmo-
492 sphere and RS99 clouds (Table 2). Albedo biases for the daytime-weighted
493 zenith angle (μ_D^* , red) and the insolation-weighted zenith angle (μ_I^* , blue) are
494 calculated relative to the absorption-weighted zenith angle (μ_A^* , black). 30

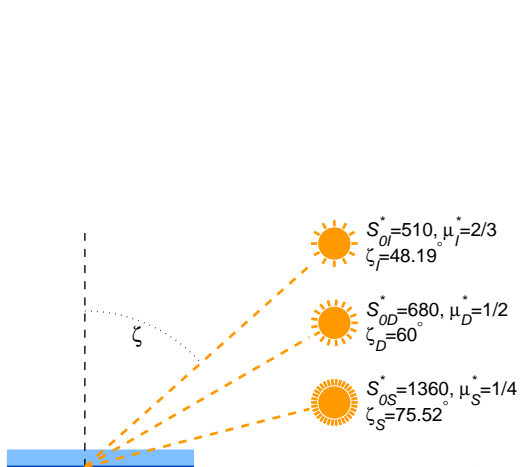


FIG. 1. Schematic example of three different choices of zenith angle and solar constant that give the same insolation. The solar zenith angle ζ is shown for each of the three choices, which correspond to simple average, daytime-weighted, and insolation-weighted choices of μ , as in the text.

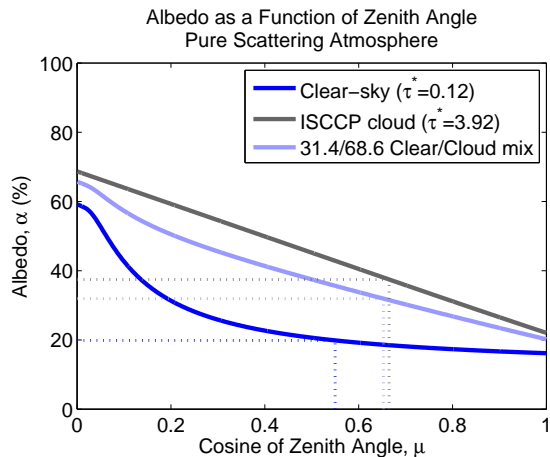


FIG. 2. Plot of albedo against cosine of the zenith angle, for a pure conservative scattering atmospheric column, based on *Pierrehumbert* (2010), equation (5.41). We show calculations for a clear-sky case with $\tau^*=0.12$ and $\hat{g}=0$ (blue), for a cloudy case, with $\tau^*=3.92$ and $\hat{g}=0.843$ (gray), and a linear mix of the two for a sky that is 68.6 % cloudy and 31.4 % clear (blue-gray). The average cloud fraction and optical thickness are taken after International Satellite Cloud Climatology Project (ISCCP) measurements (*Rossow and Schiffer* 1999), and the surface albedo is set to a constant of 0.12, independent of μ . The values of the cosines of absorption-weighted zenith angle are indicated by the x-locations of the vertical dotted lines, and the planetary-average albedos are indicated by the y-locations of the horizontal dotted lines (see also Table 1).

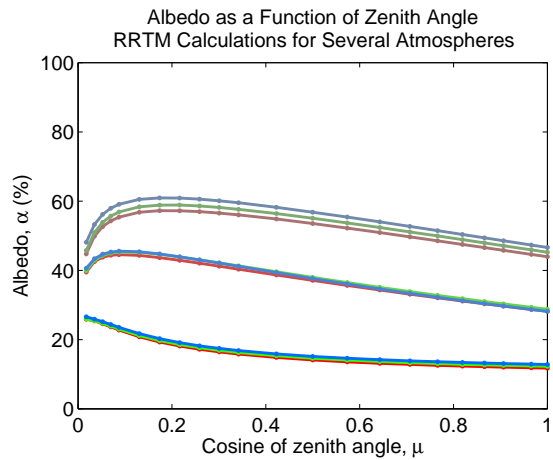


FIG. 3. Plot of albedo against cosine of the zenith angle, for calculations from RRTM. Albedo is shown for three atmospheric profiles: Tropical (red), 1976 U.S. Standard (green), and Subarctic winter (blue). We also show results for clear-sky radiative transfer (bottom set of lines), as well two cloud profile assumptions: observed RS99 cloud climatology (middle set of lines), and Stratocumulus overcast (upper set of lines) – see Table 2 for more details on cloud assumptions. The surface albedo is set to a constant of 0.12 in all cases, independent of μ .

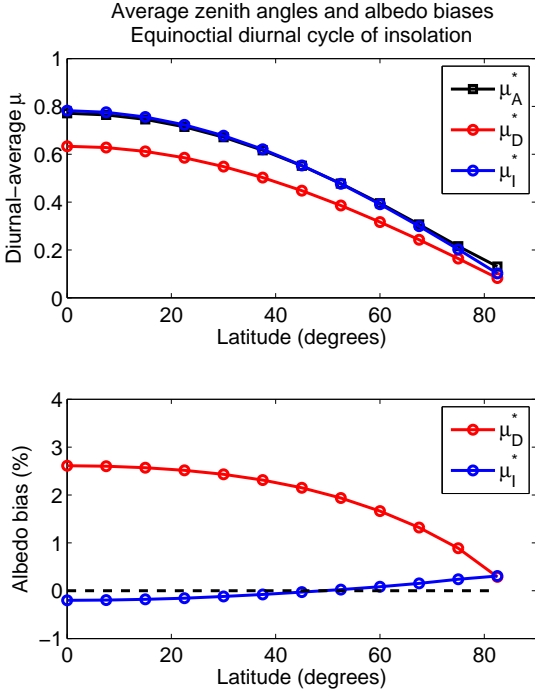


FIG. 4. Plot of diurnal-average zenith angles (top), and biases in time-mean albedo (bottom) for equinoctial diurnal cycles, as a function of latitude. Albedo is calculated in RRTM, using the 1976 U.S. Standard Atmosphere and RS99 clouds (Table 2). Albedo biases for the daytime-weighted zenith angle (μ_D^* , red) and the insolation-weighted zenith angle (μ_I^* , blue) are calculated relative to the absorption-weighted zenith angle (μ_A^* , black).

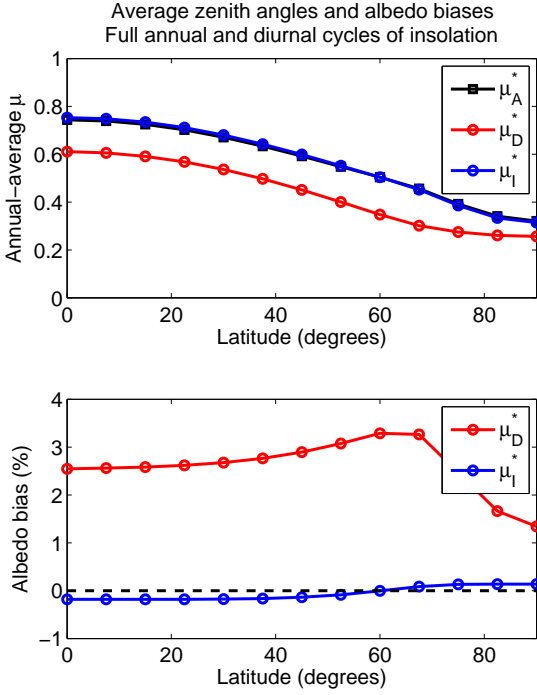


FIG. 5. Plot of annual-average zenith angles (top), and biases in time-mean albedo (bottom) for full annual and diurnal cycles of insolation, as a function of latitude. Albedo is calculated in RRTM, using the 1976 U.S. Standard Atmosphere and RS99 clouds (Table 2). Albedo biases for the daytime-weighted zenith angle (μ_D^* , red) and the insolation-weighted zenith angle (μ_I^* , blue) are calculated relative to the absorption-weighted zenith angle (μ_A^* , black).